ATMOSPHERIC SCIENCE

Ion-molecule interactions enable unexpected phase transitions in organic-inorganic aerosol

David S. Richards[1]*, Kristin L. Trobaugh[1], Josefina Hajek-Herrera[1], Chelsea L. Price[2], Craig S. Sheldon[2], James F. Davies[2], Ryan D. Davis[1†]

Atmospheric aerosol particles are commonly complex, aqueous organic-inorganic mixtures, and accurately predicting the properties of these particles is essential for air quality and climate projections. The prevailing assumption is that aqueous organic-inorganic aerosols exist predominately with liquid properties and that the hygroscopic inorganic fraction lowers aerosol viscosity relative to the organic fraction alone. Here, in contrast to those assumptions, we demonstrate that increasing inorganic fraction can increase aerosol viscosity (relative to predictions) and enable a humidity-dependent gel phase transition through cooperative ion-molecule interactions that give rise to long-range networks of atmospherically relevant low-mass oxygenated organic molecules (180 to 310 Da) and divalent inorganic ions. This supramolecular, ion-molecule effect can drastically influence the phase and physical properties of organic-inorganic aerosol and suggests that aerosol may be (semi)solid under more conditions than currently predicted. These observations, thus, have implications for air quality and climate that are not fully represented in atmospheric models.

INTRODUCTION

Accurately representing the phase of atmospheric particles (for example, liquid versus solid, phase separated versus homogeneously mixed) is important in climate and air quality models because of the influence on multiphase chemistry, aerosol water uptake and optical properties, and other atmospheric processes (*1*–*10*). Atmospheric aerosol can be composed of both inorganic components (e.g., Na^+, Cl^-, Ca^{2+}, NH_4^+, and SO_4^{2-}) and organic compounds of biogenic origin, including monosaccharides, and low-mass oxygenated compounds formed through secondary processing (*2*, *5*–*12*). The chemical complexity of atmospheric aerosol allows for particles to adopt a range of possible phase states, including nonviscous liquids, crystalline solid, or amorphous semisolid (*4*–*10*, *13*). However, the fundamental processes that govern aerosol phase remain poorly understood because atmospheric particles frequently exist under conditions inaccessible in bulk solution (*4*–*6*, *13*–*19*). Thus, the phase state of ambient atmospheric aerosol remains poorly constrained, particularly for mixed organic-inorganic aerosol (*15*, *16*, *20*).

Organic aerosol composed of relatively low-mass oxygenated organic compounds (<1000 Da), such as monosaccharides (common proxies for oxygenated aerosol material) and similar compounds, are generally assumed to remain in a liquid state or form ultraviscous or glassy Newtonian fluids at ambient relative humidity (RH) (*6*–*9*, *13*–*19*). Knowledge of aerosol viscosity is thus used to infer rates of diffusion of water or reactive species in aerosol particles through the Stokes-Einstein relationship (*6*). To a first approximation, the addition of hygroscopic salts to a homogeneously mixed organic-inorganic aerosol (e.g., a glucose-NaCl mixture) is expected to reduce the viscosity of the mixture relative to the organic alone, consistent with bulk predictions of the plasticizing effect of increased water associated with the hygroscopic salt (*15*, *16*, *18*). While this assumption is true for some cases (*15*, *16*), it has not been validated for the full range of complex compositions and nonideal conditions found in the atmosphere (*20*, *21*). In particular, the influence of divalent ions, which are prevalent in atmospheric and marine aerosol (*1*, *22*–*24*), is understudied.

Although it is known that dications such as Ca^{2+} can promote the supramolecular assembly of long-range gelatinous networks of large biopolymers (e.g., alginate, 10,000+ Da) in bulk solution (*1*, *22*, *25*), atmospherically relevant low-mass oxygenated molecules (e.g., glucose, 180 Da) do not assemble in bulk solution in the presence of Ca^{2+} (*22*). Therefore, on the basis of bulk observations, these supramolecular interactions are not considered in predictions of aerosol-phase state. However, the effect of divalent ions under the full range of conditions accessible in aerosol particles has not been adequately explored, and the RH-dependent phase state of atmospheric organic-inorganic aerosol thus remains unclear.

Motivated by the atmospheric prevalence of low-mass oxygenated organic molecules and divalent inorganic ions, we studied the RH-dependent phase state of internally mixed organic-inorganic microdroplets to test assumptions regarding aerosol phase and the effect of inorganic compounds. Experiments were performed with a dual-balance quadrupole electrodynamic balance (DBQ-EDB) technique that we recently developed specifically to explore aerosol phase (*14*). Here, we focus specifically on the RH-dependent phase of mixed organic-inorganic aerosol-containing divalent ions (Ca^{2+}, Mg^{2+}, and SO_4^{2-}) and low-mass oxygenated organics (<310 Da).

RESULTS

The phase state of levitated aerosol microdroplets was explored as a function of RH for a range of mixed organic-inorganic compositions. The organic molecules represent common atmospheric and marine aerosol proxies (*2*, *7*, *9*, *10*, *14*, *23*): glucose (the most common monosaccharide), sorbitol (a neutral sugar alcohol), gluconic acid (an aldonic acid), glucuronic acid (a uronic acid), and *N*-acetylneuraminic

[1]Department of Chemistry, Trinity University, 1 Trinity Place, San Antonio, TX 78212, USA. [2]Department of Chemistry, University of California-Riverside, Riverside, CA 92521, USA.
*Present address: University of Kansas, Department of Pharmaceutical Chemistry, 2093 Constant Avenue, Lawrence, KS 66047, USA.
†Corresponding author. Email: rdavis5@trinity.edu

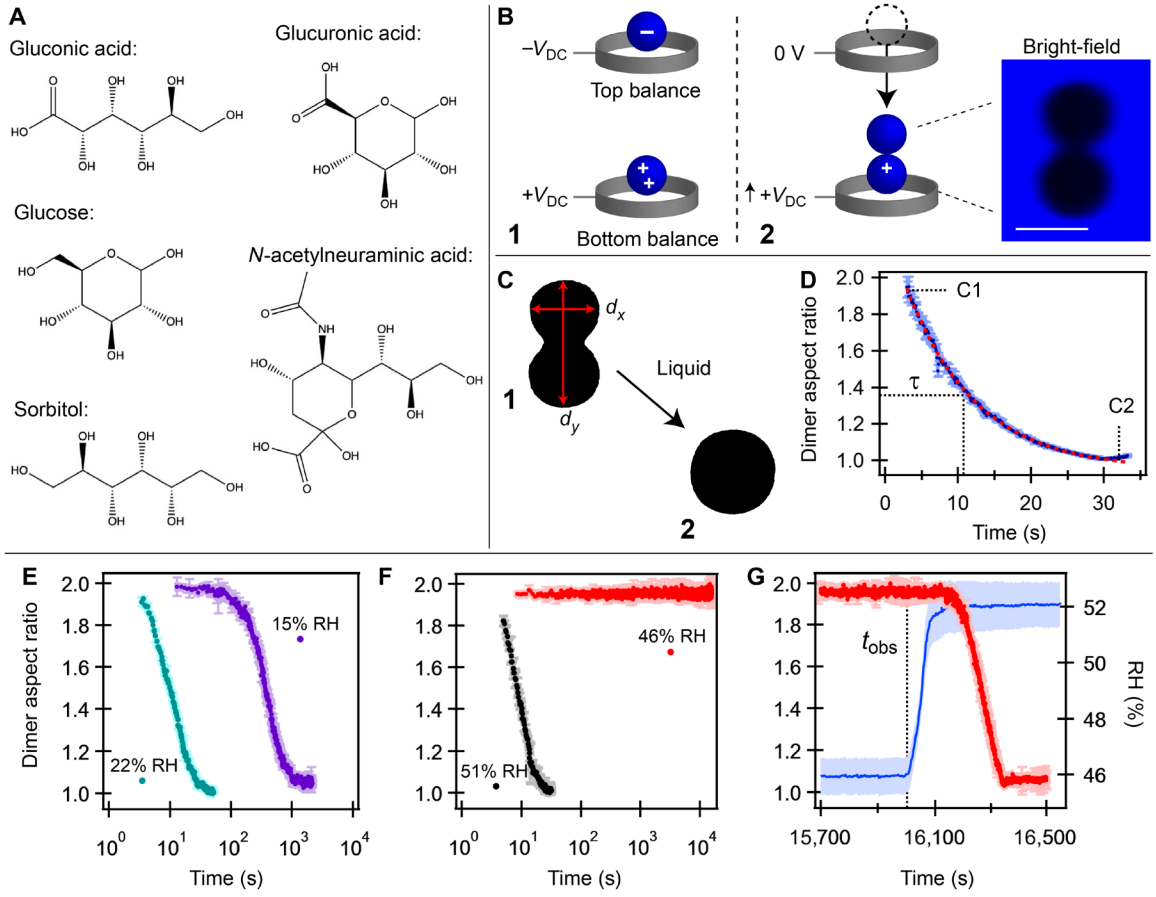

Fig. 1. Determining the phase of levitated organic and inorganic-organic particles. (**A**) The organic molecules used in the present study. (**B**) Simplified schematic of the DBQ-EDB and process of merging droplets to determine particle phase. (1) Two oppositely charged droplets of the same composition and size are simultaneously levitated. The particle in the bottom balance is continuously monitored with bright-field imaging. (2) Upon removing the voltage applied to the top balance, the droplets merge through electrostatic attraction (inset; scale bar, 30 μm). The voltage applied to the bottom balance is increased to account for the increased mass and reduced net charge. (**C** and **D**) Typical behavior of a liquid upon merging. Plotted is the aspect ratio (d_y/d_x) as a function of time for coalescence of binary gluconic acid (liquid droplets) at 15 ± 2%. Representative images are shown in (C), panels 1 and 2, as indicated. Dashed red line is the exponential fit (τ = 11.5 ± 0.3 s). (**E** to **G**) Aspect ratio as a function of time for merged ternary salt–gluconic acid droplets. (E) Merging of ternary 1:1 (by mole) NaCl:gluconic acid at a constant RH of 15 and 22% RH. (F) Two merging events for ternary 1:1 (by mole) $CaCl_2$:gluconic acid droplets at a constant RH of 46 and 51% RH. No coalescence occurs over the observation time (t_{obs}), indicating solid-like phase behavior. (G) Aspect ratio and RH as a function of time as RH (blue line) is increased for the same merged particle shown in (F) at 46% RH. In (D) to (G), each data point represents the average aspect ratio (±1 SD) of five sequential images.

acid (a sialic acid) (Fig. 1A). All five organics were systematically studied in aqueous organic (binary) droplets and aqueous organic-inorganic (ternary) droplets with either NaCl or $CaCl_2$. Ternary gluconic acid droplets were further studied with $(NH_4)_2SO_4$, $MgCl_2$, $MgSO_4$, and $Ca(NO_3)_2$. These chemical systems were chosen as simple models of mixed organic-inorganic aerosol because of their natural abundance in atmospheric and marine aerosol and their physical properties and to compare the effects of molecular functionality.

As demonstrated in Fig. 1B, droplet phase was probed using the DBQ-EDB technique (fig. S1A) (*14*) to merge two droplets of the same composition and diameter (~30 ± 2 μm), after equilibration at a constant RH for a fixed amount of time. The shape of the merged dimer was monitored as a function of time by tracking the droplet aspect ratio, d_y/d_x, where d_y and d_x are, respectively, the diameter of the long and short axes of the particle (see Fig. 1C), or by far-field laser scatter imaging (fig. S1B). As established by our work (*14*) and that of others (*15*–*18*, *26*), monitoring the coalescence process of merged droplets under variable RH conditions can provide detailed information regarding RH-dependent aerosol-phase state. The typical phase behavior of binary organic and ternary organic-inorganic droplets is exemplified with individual merging events of binary gluconic acid (Fig. 1D and fig. S1C) and ternary gluconic acid mixtures (Fig. 1, E to G). The RH-dependent results for all systems are shown in Figs. 2 and 3.

Binary H_2O-organic and ternary H_2O-NaCl–organic droplets remain as liquids

For binary organics, the expected RH-dependent phase is observed in all cases, as demonstrated with the coalescence of binary gluconic acid droplets at ~15% RH (Fig. 1D) and 10% RH (fig. S1C). As seen in Fig. 1D, upon merging at 15% RH, the bispherical dimer exponentially relaxes to a spherical shape with a time constant (τ) of ~10 s. This gradual relaxation is consistent with the overdamped regime of a viscous Newtonian fluid, where τ is directly proportional to viscosity of the fluid [see the "Relating shape relaxations to phase"

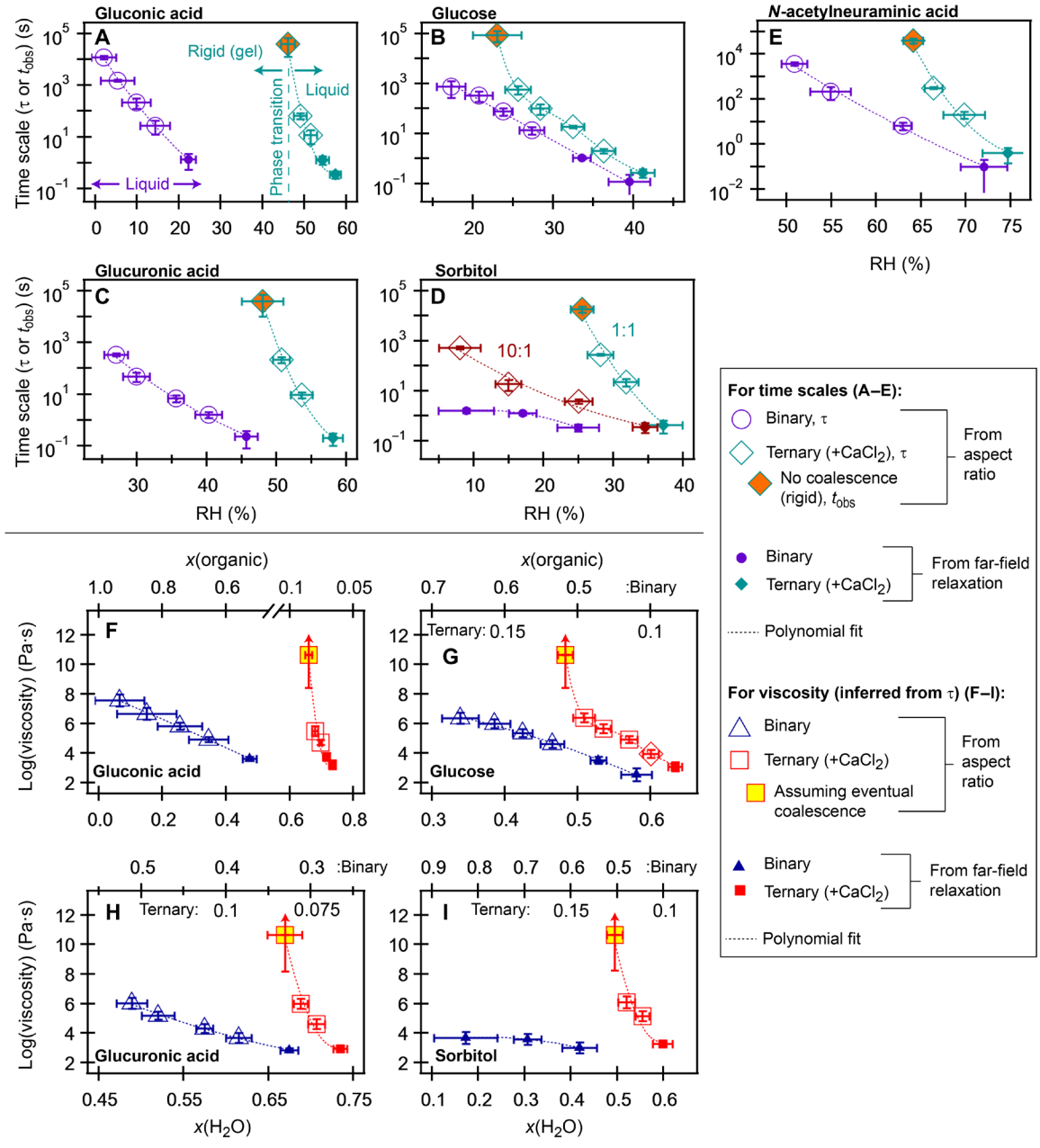

Fig. 2. Experimental results for the merging of binary and ternary $CaCl_2$-organic droplets. (**A** to **E**) RH-dependent time scales. If coalescence was observed, then average τ (±1 SD) is reported. If no coalescence was observed and merged dimers were rigid, then average t_{obs} (±1 SD) is reported. The organic component is indicated in each panel. Polynomial fits are shown to facilitate the comparison of trends in data. Each data point represents the average (±1 SD) of at least five trials (A to D, except binary gluconic acid at 2% RH) or three trials (E, and binary gluconic acid at 2% RH). The data for binary glucose are adapted from (*14*). In (A), the transition from liquid to rigid gel is indicated with the vertical dashed line. (**F** to **I**) The RH-dependent time scales were converted to inferred viscosity and plotted as a function of water mole fraction (bottom axis) and organic mole fraction (top axis) for gluconic acid, glucose, glucuronic acid, and sorbitol, as estimated with AIOMFAC. (*N*-acetylneuraminic acid cannot be adequately defined in AIOMFAC to account for interaction with ions, and the results were therefore not converted to water mole fractions; see fig. S2 for the viscosity of *N*-acetylneuraminic acid versus RH.) For rigid gels, the τ values were estimated from fig. S3 assuming Newtonian behavior, using a τ value of 1×10^7 s, with the lower limit to the error bars representing the experimental t_{obs}. The upper limit to viscosity is not known.

section in the Supplementary Materials for additional details] (*17*). Upon decreasing RH to ~10%, binary gluconic acid droplets coalesce on longer time scales (τ ≈ 100 s), as shown in fig. S1C. This increase in τ with decreasing RH is consistent with expectations of the plasticizing effect of water, where viscosity, and thus τ, increases gradually with decreasing RH due to decreasing water content (*14*–*19*). As seen in Fig. 2A, τ indeed increases consistently, as RH is decreased from ~20 to 2%, with approximately one–order of magnitude increase in τ for every 5% decrease in RH. As seen in Fig. 2 (A to E), all binary organic systems exhibited similar RH-dependent behavior,

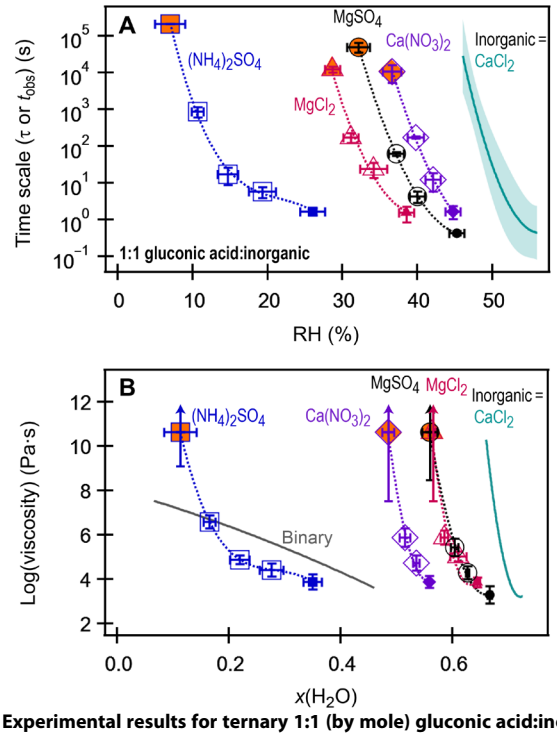

Fig. 3. Experimental results for ternary 1:1 (by mole) gluconic acid:inorganic droplets. All inorganic salts contain at least one divalent ion. The identity of the inorganic salt is indicated on the figure. (**A**) RH-dependent time scales. For 1:1 gluconic acid:$CaCl_2$, the polynomial fit to the data shown in Fig. 2A is plotted here. Open symbols indicate data from the bright-field aspect ratio. Closed symbols indicate data from the far-field relaxation. Orange-filled symbols indicate no coalescence (presumed gel). Each data point represents the average (±1 SD) of at least three trials. (**B**) Inferred viscosity plotted as a function of water mole fraction (as estimated with AIOMFAC). For rigid gels, the τ values were estimated from fig. S3 assuming Newtonian behavior, using a τ value of 1×10^7 s, with the lower limit to the error bars representing the experimental t_{obs}. The upper limit to viscosity is not known.

consistent with expectations (*14*–*19*). Of these organics, only binary *N*-acetylneuraminic acid is expected to undergo a clear glass transition at low RH [~25% RH if extrapolated from fig. S2 to a viscosity of 10^{12} Pa·s or ~5%, as estimated with AIOMFAC (Aerosol Inorganic-Organic Mixtures Functional groups Activity Coefficients) (*27*); see Materials and Methods for details]; RH-induced glass transitions are not typically observed for the lower-mass oxygenated molecules such as glucose (*14*, *17*, *19*), consistent with our observations.

When NaCl is present in ternary 1:1 (by mole) NaCl:organic droplets, the observed RH-dependent trend is similar to that of binary organics, with a gradual increase in τ (and viscosity) as RH is decreased, as demonstrated in Fig. 1E for 1:1 NaCl:gluconic acid droplets. Here, τ increases from ~10 s at 22% RH to ~300 s at 15% RH. In general, as seen in fig. S2, NaCl reduces or has a minor influence on viscosity, consistent with expectations of the plasticizing effect of the water associated with the hygroscopic NaCl (*15*, *16*) and the Na^+:COO^- interaction (*28*) (see the "Expectations from mixing approximations" section in the Supplementary Materials for additional discussion). Although the presence of NaCl altered the time scale of coalescence and viscosity relative to the binary systems, the phase behavior of the NaCl-organic systems did not deviate from that expected of Newtonian fluids.

Ternary H_2O-$CaCl_2$–organic droplets have elevated viscosity and can spontaneously transition to a rigid, gel phase state

Relative to binary and ternary NaCl droplets, very different phase behavior was observed for ternary 1:1 (by mole) $CaCl_2$:organic droplets. Figure 1F demonstrates examples of merging ternary $CaCl_2$:gluconic acid droplets at a constant RH of ~51 and 46%. At ~51% RH, merged droplets completely coalesced with $\tau \approx 10$ s. Notably, τ at 51% RH was similar to that of 1:1 NaCl:gluconic acid at ~22% RH (Fig. 1E). However, upon decreasing RH by ~5% and merging at 46% RH, no coalescence was observed and merged droplets remained completely rigid at constant RH over an observation time (t_{obs}) of 16,000 s. This t_{obs} at 46% RH is three orders of magnitude larger than the observed τ at 51% RH, thus demonstrating an abrupt change in phase from fluid- to solid-like behavior across a narrow RH range. With no observable decrease in aspect ratio over a long time scale, τ could not be directly determined for merging events such as that shown in Fig. 1F at 46% RH. Thus, in these cases, t_{obs} is reported in Fig. 2 (A to E). (Attempts to determine τ by assuming an eventual decay of aspect ratio to unity resulted in estimated values of τ ranging from 10^7 to 10^{13} s, as shown in fig. S3.) As seen in Fig. 1G, the rigid structure disassembles upon increasing RH, indicative of a phase transformation. As seen in Fig. 2A, rather than a gradual change in time scale, as observed with the binary organics, the change in phase behavior is abrupt.

Converting time scales to viscosity (Fig. 2F) demonstrates that ternary gluconic acid–$CaCl_2$ droplets have a much higher viscosity, relative to binary gluconic acid, despite also having a much higher water mole fraction, $x(H_2O)$, and lower organic mole fraction [as estimated with AIOMFAC (*29*)]. (The range of potential viscosity values for rigid particles was constrained, assuming Newtonian behavior with eventual coalescence and a τ value of 10^7 s, as described in fig. S3.) For example, ternary $CaCl_2$–gluconic acid and binary gluconic acid droplets exhibit a comparable viscosity (~10^5 Pa·s) at, respectively, ~51 and 14% RH, despite the ternary system having substantially more water [$x(H_2O) \sim 0.7$ compared to ~0.35] and less organic [x(gluconic acid) ~ 0.075 compared to ~0.65]. This behavior cannot be explained using simple viscosity mixing estimates (discussed more in the "Expectations from mixing approximations" section in the Supplementary Materials), nor can it be explained by liquid-liquid phase separation (LLPS) and efflorescence (as discussed in fig. S4), and this indicates that the underlying microstructure is changed with the combination of gluconic acid and $CaCl_2$. This abrupt change in phase (fig. S5A), along with increased water content (as confirmed with Raman spectroscopy in fig. S5B), is consistent with (hydro)gel formation, i.e., formation of a two-phase combination of liquid (water) contained within a porous solid network that assembles and disassembles within a relatively narrow range of solute concentration (*1*, *13*, *14*, *30*, *31*).

All ternary 1:1 $CaCl_2$:organic systems exhibited similar RH-dependent behavior, as shown in Fig. 2 with individual examples shown in fig. S6. That is, an increase in viscosity (relative to the binary systems) and an abrupt transition to a rigid phase where droplets did not coalesce over long observation times, consistent with a gel transition (*14*) (see the Further evidence for a gel phase transition section in the Supplementary Materials for additional discussion). In these instances, a transition from $\tau \approx 10^2$ s to $t_{obs} >> 10^4$ s (viscosity ≈ 10^5 Pa·s to estimated viscosity > 10^{10} Pa·s) occurred within a decrease of 2 to 3% RH or less. The effect was perhaps most pronounced with sorbitol (Fig. 2, D and I). Binary sorbitol and binary

$CaCl_2$ remain relatively nonviscous under dry conditions (*14*, *32*), whereas ternary 1:1 $CaCl_2$-sorbitol was rigid at ~26% RH. Of the other ternary $CaCl_2$-organic combinations, $CaCl_2$–*N*-acetylneuraminic acid exhibited a rigid structure at the highest RH (~64%), while $CaCl_2$-gluconic and $CaCl_2$–glucuronic acid became rigid at ~46 and 48% RH, respectively, and $CaCl_2$-glucose was rigid at ~22% RH. In bulk solution, these systems are not expected to undergo gel phase transitions (*22*, *33*). However, aerosol particles can reach high levels of supersaturation, thus facilitating transitions not observed in bulk (*13*, *14*, *24*).

The effect of $CaCl_2$ is also clearly demonstrated in 10:1 (by mole) sorbitol:$CaCl_2$. As seen in Fig. 2D, although no rigid gel transition is observed (at RH ≥ 8%), the presence of $CaCl_2$ increases the coalescence time scale (and thus viscosity) of sorbitol, even at low $CaCl_2$ concentrations. At ~8% RH, the ternary 10:1 system has a viscosity [$2.0(\pm0.9) \times 10^6$ Pa·s] that is greater than sorbitol alone under completely arid conditions [$5(\pm2) \times 10^4$ Pa·s] (*14*). This demonstrates that, even in the absence of a distinct gel phase transition, low concentrations of divalent inorganic compounds can increase aerosol viscosity and influence the phase of organic-inorganic aerosol.

Gel phase transitions can occur in the presence of a range of divalent ions

To further explore the generality of the observed rigid transition, we probed for phase transitions of gluconic acid in the presence of a range of inorganic compounds containing divalent ions. As shown in Fig. 3A, an RH-dependent transition, consistent with a gel transition, is observed in 1:1 (by mole) mixtures of gluconic acid with $Ca(NO_3)_2$, $MgCl_2$, $(NH_4)_2SO_4$, and $MgSO_4$. The effect is most pronounced with Ca^{2+} and least pronounced when only a divalent anion is present [i.e., $(NH_4)_2SO_4$]. As seen in Fig. 3B, the RH at which the rigid transition is observed is related to water content. Notably, when the inorganic compound is $MgCl_2$ or $MgSO_4$, the ternary droplets become rigid at a nearly identical water mole fraction (~0.6), suggesting that the effect is dominated by the dication. However, as suggested by the differing water content of $CaCl_2$ and $Ca(NO_3)_2$ rigid gels, the anion does influence the phase transition. In the case of $(NH_4)_2SO_4$, ternary mixtures are initially less viscous than binary gluconic acid until low water content. By contrast, the ternary mixtures containing dications were more viscous than the binary droplets at all RH (water mole fractions) studied. Although the identity of the divalent ion and counterion shifts the RH at which gelation was observed, an apparent gel transition was observed in all cases, suggesting that the possibility of gel formation from highly oxygenated organics is a general effect in the presence of divalent ions, and that the threshold RH is likely dictated by water content and thus solvation structure of the ions and molecules involved.

Aerosol water transport is slowed in ternary $CaCl_2$-organic droplets

Distinguishing between liquid and gel states is particularly important for understanding transport and partitioning of particle-phase water. As shown in fig. S5B using Raman spectroscopy, there remains a significant amount of water present in the ternary droplets at an RH below the observed rigid transition, consistent with predictions from thermodynamic models (see table S1) (*28*). Increased water content coincident with increased rigidity (relative to the binary systems) is strong evidence for a (hydro)gel transition (*14*, *31*). The elevated water content also confirms that no efflorescence transition occurred, consistent with observations from laser scatter imaging and droplet mass measurements (fig. S4, B and C). To explore the nature of this water, we measured the rate of water transport using the RH oscillation approach of Preston *et al.* (*34*) in a linear quadrupole EDB using Mie resonance spectroscopy (*35*). Figure 4A shows that slow reversible water transport occurs in $CaCl_2$-sorbitol ternary droplets below the gel transition RH, and the time scale for water transport increases sharply as RH decreases (Fig. 4B).

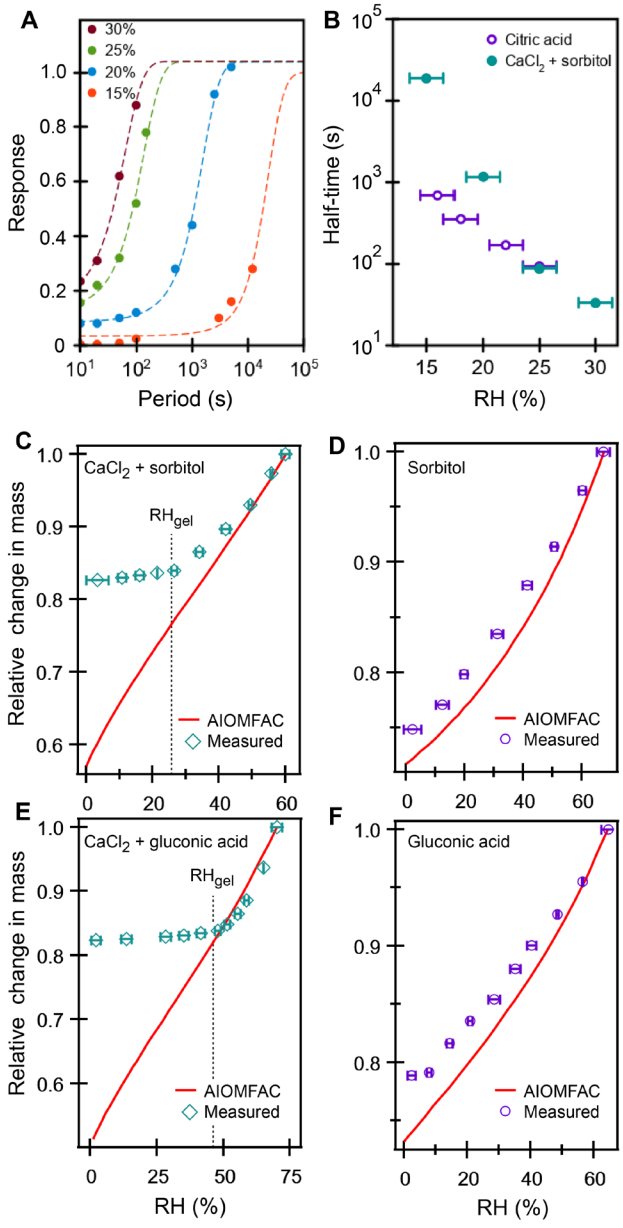

Fig. 4. Hygroscopic response to binary and ternary droplets. (**A** and **B**) Response to RH oscillations for 1:1 $CaCl_2$:sorbitol droplets. (A) Droplet response to oscillations in RH. A sigmoid function was fit to the data (dash lines) to determine the half-time, shown in (B). (B) Half-time as a function of RH. Droplet response below the gel formation RH (<25% RH) is very slow, and the maximum amplitude was estimated on the basis of the response at higher RH. Data for citric acid from Preston *et al.* (*34*) are shown for comparison. (**C** to **F**) Relative mass of single droplets, as measured in the DBQ-EDB, compared to AIOMFAC predictions for (C) ternary 1:1 $CaCl_2$:sorbitol, (D) binary sorbitol, (E) ternary 1:1 $CaCl_2$:gluconic acid, and (F) binary gluconic acid.

Substantial slowing below an RH of 20 to 25% is observed, consistent with the RH range where coalescence measurements indicate transformation to a rigid gel structure. Compared to the increase in time scale for binary citric acid (a viscous fluid that exhibits time scales at 25% RH that are similar to the $CaCl_2$-sorbitol system), this slowing is much more abrupt and indicative of a phase transformation rather than a continuous change in viscosity.

To further establish the water transport behavior in these systems, we examined the single-particle relative change in mass as a function of RH for sorbitol and gluconic acid systems and compared that to predictions from AIOMFAC. As RH is decreased, there is a loss of particle-phase water to maintain equilibrium, which is evident by a decrease in mass of levitated droplets. As seen in Fig. 4C for a 1:1 $CaCl_2$-sorbitol droplet, there is an abrupt slowing in loss of particle-phase water below ~25%, consistent with the RH_{gel} identified through coalescence measurements. By contrast, no abrupt slowing is seen in binary sorbitol (Fig. 4D) or binary $CaCl_2$ (fig. S4C). Similar slowing, indicative of diffusive limitations, is seen in ternary $CaCl_2$–gluconic acid (Fig. 4E) droplets at ~45 to 50% RH, consistent with the identified RH_{gel} for this system. Binary gluconic acid droplets (Fig. 4F), however, exhibit no significant diffusive limitations until very low RH. These measurements confirm that the ternary $CaCl_2$-organic systems are more rigid and more resistant to water transport than the binary systems alone.

The exact mechanisms of water transport in these systems are not yet resolved; percolation through a porous network and viscous flow must be considered to fully explain the observed dynamics. However, these observations are consistent with previous observations of water diffusion in porous gels (*13*), supporting the assertion that a gel transition occurs and demonstrating the slow mass transport dynamics in these systems.

The observed phase transition and increased viscosity in ternary systems is an emergent process enabled by supramolecular ion-organic interactions

The increased viscosity and phase transformation to a rigid gel in ternary systems with divalent ions, as observed here, must be a result of cooperative interactions between the ions and the organics, as evident from the fact that gelation is not promoted by ion-ion (or solute-solute) interactions in binary inorganics (or binary organics). Figure 5A shows the RH at which rigid gelation was observed (RH_{gel}) for each 1:1 $CaCl_2$-organic mixture as a function of molecular weight (of the organic) with the main functional groups of each molecule indicated in the figure. Hydroxyl (OH) groups are common to all of the organic compounds. As shown in Fig. 5B, the identity of both the cation and anion influences RH_{gel}. We thus propose that the gel network develops through pairing of the established ion-organic complexes that form in bulk solution via ion-OH interactions (Fig. 5C) (*36*–*39*). In bulk solution, and in microdroplets at $RH > RH_{gel}$, individual ion-organic complexes remain separate and well solvated. As water content is reduced with decreasing RH, there is inadequate water to fully solvate all solutes (*4*), and we propose that long-range networks develop through extensive, supramolecular contact ion pairing of the ion-molecule complexes, e.g., $[Ca^{2+}{\cdot}C_6H_{14}O_6{\cdot}Cl^{-}{}_2]_n$, creating the semisolid gel network (Fig. 5D).

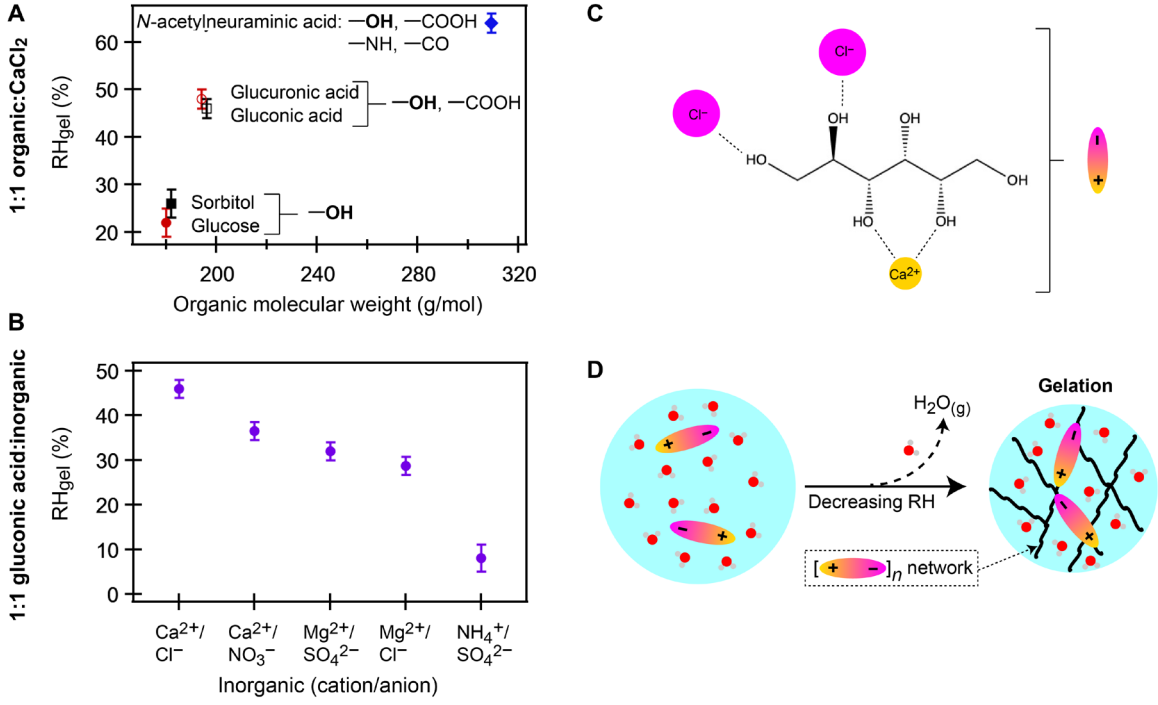

Fig. 5. The proposed pathway for supramolecular assembly of gels in aerosol particles. (**A** and **B**) The chemical factors influencing the gel phase transition. (A) RH_{gel} for the ternary $CaCl_2$-organic mixtures plotted as a function of organic molecular weight. The main molecular functional groups for each organic are indicated on the plot. (B) RH_{gel} for ternary gluconic acid–inorganic mixtures graphed as a function of inorganic cation/anion. (**C** and **D**) Proposed pathway for assembly from neutral organics in the presence of Ca^{2+}. (C) An example of an ion-sorbitol complex that could act as the monomer units. Other conformations are also possible (*37*). (D) Illustration demonstrating a potential pathway for gelation with decreasing RH. At high RH (left), monomer units are fully solvated and separated. With decreasing RH, water content is reduced and long-range networks can form through contact ion pairing (right).

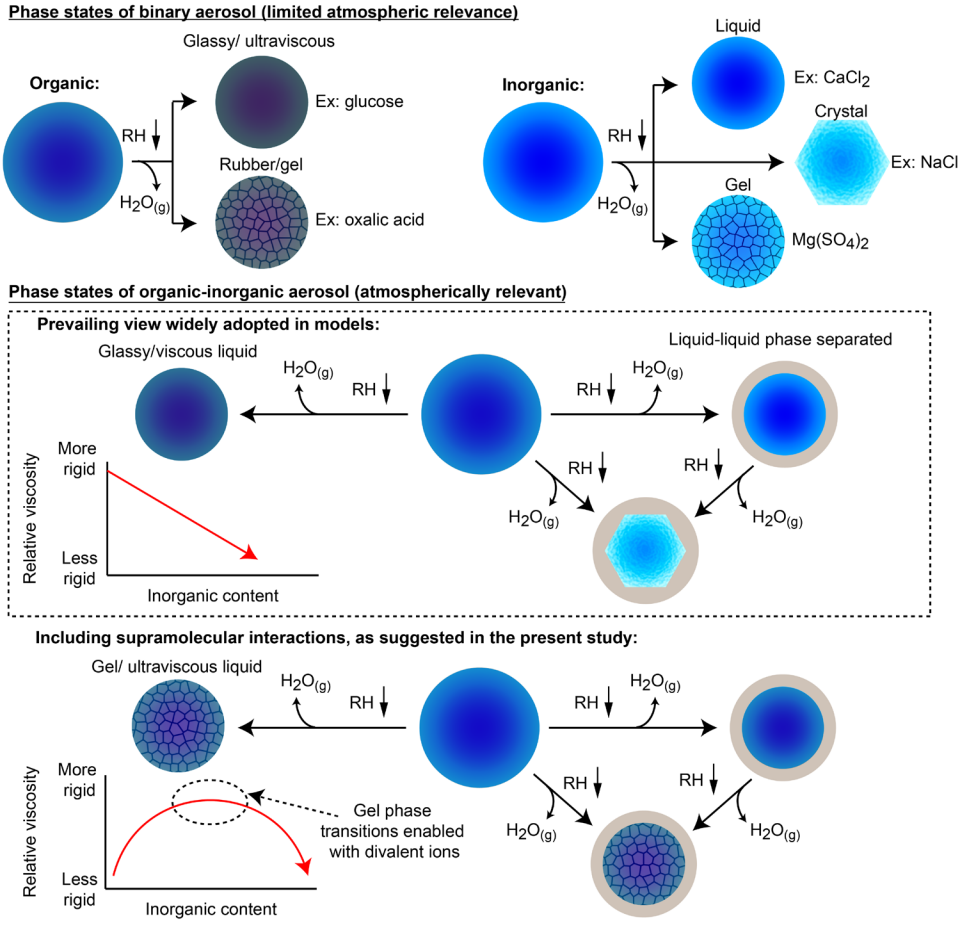

Fig. 6. Potential phase states of aqueous aerosol particles upon decreasing RH. (**Top**) Established, well-studied phase states of binary oxygenated organic and binary inorganic aerosol. Binary organics most commonly remain liquid and gradually increase in viscosity to form a glassy or ultraviscous phase (*17*). Binary inorganic compounds commonly will homogeneously effloresce (crystallize with loss of particle-phase water) (*4*), although there are multiple examples of aqueous inorganics that do not homogeneously effloresce at all or not until very low RH (<1%) (for example, $CaCl_2$, $NaNO_3$, and NH_4NO_3) (*5*). Gel transitions have been observed in a limited number of cases (*5*, *13*, *14*). Binary aerosol phase transitions are essential for establishing fundamental understanding but have limited atmospheric relevance because of the complexity of atmospheric aerosol. (**Middle**) Prevailing view of phase transitions relevant to mixed organic-inorganic aerosol. LLPS can occur, typically with less oxygenated organics (O:C < ~0.5) comprising the outer shell and aqueous inorganics remaining in the core (*10*). After LLPS, the inorganic fraction can effloresce upon further decrease in RH. Particles that remain homogeneously mixed can partially effloresce or remain homogeneously mixed and gradually increase in viscosity as RH is reduced (*5*, *10*, *15*). For homogeneously mixed organic-inorganic aerosol, it is widely assumed that increasing inorganic content will reduce viscosity through the plasticizing effect of the water associated with the hygroscopic salt (*15*, *16*). However, as shown in the present study and illustrated in (**bottom**), inorganic compounds can increase organic-inorganic aerosol viscosity and promote aerosol gel transitions through supramolecular, ion-molecule interactions. This supramolecular effect is not represented in current models. Considering that LLPS does not inhibit efflorescence of an aqueous inorganic core (*10*), we posit that LLPS will not inhibit the supramolecular effect in complex aerosol where the core likely contains aqueous inorganics in addition to highly oxygenated organics.

In this proposed gelation pathway, cross-linking is enabled by the divalent ion (*1*, *13*, *14*, *22*, *31*, *33*), analogous to the mechanism by which binary $MgSO_4$ gelation occurs (*13*, *24*). The carboxylic acids may have had the highest gelation RH due to Ca^{2+} chelation, effectively forming a disaccharide (fig. S7A), and thus a higher RH_{gel} through the established connection between increasing monomer size and increased gelation ability (*1*, *22*, *33*). In the 10:1 sorbitol:$CaCl_2$ system, viscosity was higher than binary sorbitol, but a distinct gel transition was not observed in the RH range studied. In this instance, it is likely that there was insufficient Ca^{2+} to form long-range networks, but short-range Ca-sorbitol chains still develop that increase viscosity (fig. S7B). These observations suggest that even in the absence of a distinct, long-range gel transition, short-range supramolecular units can still form that increase the effective viscosity of organic-inorganic aerosol, possibly resulting from the established link between viscosity and molecular weight (*19*).

The correlation between gel transition and particle-phase water content supports the idea of ion pairing mediated by ion-molecule complexes. Examining the water content of ternary $CaCl_2$ mixtures (for which gelation was observed and thermodynamic data were available) (Fig. 2, F to I) indicates that gelation occurs at water mole fractions of ~0.5 for neutral organics and ~0.65 for carboxylated organics. At these mole fractions, there is insufficient water to fully solvate all ions; in bulk solution, fully solvated Ca^{2+} will have six water molecules in its first solvation shell (*40*), whereas at $x(H_2O) = 0.5$, there is approximately four water molecules per Ca^{2+}. Under these low-water conditions, extensive ion pairing is possible (*24*). Similar trends in water content are observed in Fig. 3B for

Mg^{2+}. Unlike Ca^{2+} and Mg^{2+}, SO_4^{2-} prefers to remain solvated and does not readily bind to macromolecules (*41*), which could explain the very low water content necessary before the transition to a rigid phase in $(NH_4)_2SO_4$–gluconic acid droplets. Further evidence for the proposed ion pairing mechanism can be seen in RH-dependent changes to the Raman spectrum of $CaCl_2$– and $MgSO_4$–gluconic acid mixtures (fig. S8) that suggest changes to COO^- and SO_4^{2-} due to ion pairing (*24*, *40*). This evidence for ion-molecule interactions supports the concept of a gel transition in the equimolar mixtures, where the transition is promoted by the balance of attractive and repulsive forces between solutes (*30*). This differs from a glass transition, where there is no long-range solute-solute interactions (*9*). When the divalent concentration is too low to enable long-range cross-linking, we posit that short-range coupling (for example, fig. S7B) can promote a glass transition at lower RH, as suggested with 10:1 sorbitol:$CaCl_2$. In either scenario (gel or glass transition), ion-molecule interactions are promoting phase transitions when current understanding would have predicted that the inorganic content would have inhibited these transitions (*15*, *16*).

Under bulk conditions, these ion-organic complexes responsible for gelation may ultimately crystallize when water content is decreased (*42*). However, in microdroplets, crystal nucleation is inhibited (*4*). This creates a unique environment through which organics can assemble into gels through cooperative, supramolecular interactions with divalent ions under atmospherically relevant conditions in aerosol particles.

DISCUSSION

We have demonstrated a previously unexplored supramolecular, ion-molecule effect on aerosol phase under atmospherically relevant conditions not readily accessible in bulk solutions. Supramolecular ion-molecule interactions have been shown here to promote a gel phase transformation where two compounds, which were non-viscous and non-gelling as aqueous binary systems, synergistically enabled gelation when combined in mixed aqueous inorganic-organic aerosol microdroplets. Further, in the absence of any specific phase transition, this supramolecular effect was shown to increase the viscosity of mixed organic-inorganic aerosol relative to bulk predictions. Thus, gelation and vitrification through ion-molecule interactions could influence hygroscopicity and reactivity of atmospheric aerosols, with impacts on air quality and climate that is not represented in current atmospheric models.

As illustrated in Fig. 6, aerosol particles can adopt a wide range of phase states through various RH-induced phase transitions. Although it is known that gel transitions can occur in bulk organic-inorganic systems [for example, marine microgels (*1*, *22*, *33*)], gel transitions specific to aerosol have only been observed in a limited number of binary systems [for example, binary oxalic acid (*5*) and binary $MgSO_4$ (*13*, *14*, *24*)], which have limited atmospheric relevance because binary aerosol are rare in the atmosphere. For mixed organic-inorganic aerosol, the prevailing view is that, as RH is continuously decreased, organic-inorganic aerosol can either undergo LLPS, partially effloresce, or remain homogeneously mixed with a gradual increase in viscosity (*6*, *10*, *15*, *16*). For the case of homogeneous mixtures (as used in the present study), the assumption has been that with increasing inorganic content, the viscosity of the aerosol is reduced because of increased water content (*15*, *16*). However, as we have demonstrated here, supramolecular interactions between oxygenated organic and inorganic ions can lead to increased aerosol viscosity, despite elevated water content, and enable gel transitions in organic-inorganic aerosol. Supramolecular interactions will most likely be strongest when the organic compounds contain a carboxylic acid (*40*) and vicinal hydroxyl groups (*37*), which can be common in atmospheric organic compounds because of oxidative aging (*11*) and primary emission (*12*) (see the "Generalizations and parameterization" section in the Supplementary Materials for further discussion). Such compounds typically have a higher oxygen-to-carbon atom ratio [O:C; which is commonly used in atmospheric chemistry to parameterize certain aerosol properties (*11*)] and are thus less likely to undergo LLPS (*10*). We therefore posit that while phase-separated organics are less likely to be influenced by ion-molecule effects, LLPS will not inhibit these supramolecular interactions in the aqueous core of phase-separated organic-inorganic aerosol. This supramolecular effect on aerosol phase is not currently represented in atmospheric and climate models, which suggests that aerosol viscosity and phase, and thus diffusion coefficients, may be overpredicted under many conditions.

Gels exhibit different physicochemical properties than viscous fluids and thus have unique atmospheric implications (*5*, *13*, *14*). For example, diffusion coefficients of particle-phase water and reactive species can be overpredicted by several orders of magnitude if gelation occurs but is not considered (see the "Estimating the impact of supramolecular effects on diffusion constants" section in the Supplementary Materials), which is particularly notable considering that many atmospheric models assume that all particles remain as liquids (*43*). In addition, droplets of some organic-inorganic gel-forming mixtures may consist of multiple, discrete regions with differing diffusivities (for example, an aerosol particle composed of microgels embedded within a fluid matrix) and thus exhibit non-Newtonian fluid behavior (*14*, *44*). Furthermore, because we observed a supramolecular effect that increased aerosol viscosity relative to what was predicted, diffusion coefficients may be lower than would be predicted without considering ion-molecule interactions, even in the absence of (or before) a distinct phase transition. That is, the supramolecular effect on aerosol properties likely extends across a wide range of compositions and conditions.

We have further demonstrated that the observed ion-molecule effect and resulting gel transition influences aerosol hygroscopicity by inhibiting water uptake and loss. Our results are consistent with and can explain previously reported hygroscopicity observations of mixed $Ca(NO_3)_2$–malonic acid aerosol particles (*45*) and physical changes in aqueous $(NH_4)_2SO_4$–organic aerosol upon uptake of isoprene epoxydiols (*46*). Further, considering the prevalence of divalent ions in ambient atmospheric aerosol, supramolecular effects may be contributing to the observed semisolid state of atmospheric secondary organic aerosol (*47*). As a whole, these studies suggest that supramolecular effects on phase may play a role in not only aerosol hygroscopicity but also mixing time scales, reactivity, and other processes. This highlights a need to understand microstructure and phase in addition to aerosol composition to account for supramolecular ion-solute interactions when predicting aerosol properties for implementation in atmospheric and climate models.

While the study of these systems was motivated by understanding atmospheric chemistry, the divalent ion-organic interactions in aerosol particles can also be leveraged as a soft matter tool for creating supramolecular assemblies from environmentally benign compounds.

Further work remains to be done to characterize gel transitions in more complex mixtures, to validate the assembly pathway, and to model the transport of water and other species in porous gels. However, considering that we have demonstrated a gel phase transition as high as ~65% RH with relatively low-mass molecules, our results demonstrate supramolecular effects can have a profound effect on the phase and properties of atmospherically relevant organic/inorganic components under tropospheric conditions, strongly suggesting that these transformations are occurring in ambient atmospheric aerosol. Thus, further knowledge of supramolecular interactions and gel transitions outside of bulk conditions appears necessary to accurately model aerosol reactivity and hygroscopicity and, therefore, climate and human health impacts.

MATERIALS AND METHODS

Experimental design

Gel transitions were identified in a DBQ-EDB (fig. S1A). The dual-balance design is described elsewhere (*14*) along with the experimental approach used for identifying gel transitions and inferring viscosity (*14*). All experiments were conducted at room temperature (295 ± 2 K). Time scales (τ for fluids that coalesced or t_{obs} for gels that did not coalesce) were used to differentiate between RH-dependent behavior of viscous fluids (a gradual thickening) and gel formation (an abrupt transition) (*14*). To perform an experiment at a constant RH, two oppositely charged droplets (30 ± 2 μm in average diameter) of the same composition were simultaneously levitated and equilibrated [a fixed equilibration time of 5 min was used, which limited the chances for obfuscating gel and glass transitions and limited variation in extracted τ values (*14*)]. Droplets are initially generated at a bulk concentration of 5 weight % (wt %). Upon injection into the DBQ-EDB, droplets lose water to maintain an equilibrium water activity with the gas phase. The concentration of the solutes increases with decreasing RH. After the equilibration time, droplets were merged and either far-field or bright-field images were collected. Images were post-processed to determine τ or t_{obs}. When coalescence was not observed, t_{obs} was a minimum of 10^4 to 10^5 s, with bright-field images continually or intermittently collected. If aspect ratio did not decrease over this time frame, then a merging event was considered to have shown "no coalescence."

Time scales were converted to viscosity through the relationship $\tau \approx \eta r/\sigma$, where η is the viscosity, σ is the surface tension of the droplets, and r is the radius of the relaxed sphere (in all experiments, r = 18 ± 2 μm) (*14*, *17*). For binary organic and ternary organic-inorganic droplets, surface tension was estimated as 55 ± 30 and 80 ± 30 mN m^{-1}, respectively. For rigid particles where coalescence was not observed, τ values were estimated as 1×10^7 s, as shown in fig. S3, by assuming Newtonian behavior (that is, a single-exponential coalescence process) and eventual coalescence.

Electrostatic levitation

The DBQ-EDB is described in greater detail elsewhere (*14*). In brief, the DBQ-EDB is a linear quadrupole design with two counterbalances for simultaneously levitating two microdroplets. Droplets were generated using piezoelectric droplet dispensers (50-μm diameter; MicroFab MJ-ABP-050) and injected into the DBQ-EDB through an induction electrode (<±400 V_{DC} typical) to charge the droplets. Charged droplets were confined radially by a quadrupole (V_{AC} = ±600 V, 300 Hz typical) and supported vertically by the counterbalance electrodes (<±500 V_{DC} typical). The dual-balance system allowed two droplets to be equilibrated simultaneously in a humidified nitrogen flow [~500 sccm (standard cubic centimeter per minute) of total flow, typical]. Droplets were oppositely charged, and the magnitude of the charge induced on the droplet that was levitated in the top balance was less than the particle that was levitated in the bottom balance. Thus, the merged droplet contained enough charge to remain levitated in the bottom balance after merging. The RH in the DBQ-EDB was controlled by varying the ratio of dry and humidified nitrogen gas flows. Calibrated RH sensors (Honeywell HIH-4602-C) were placed before and after the DBQ-EDB, and the RH within the chamber was determined as the average of the two sensors (±1 SD, ~1% RH typical).

Imaging of merging events

Bright-field imaging was used to determine the aspect ratio of merged droplets as a function of time at long time scales (>3 s) (Fig. 1C and fig. S1C). Upon merging, the merged dimer was inadvertently removed from the field of view of the imaging cameras because of the change in mass and charge. The merged dimers were brought back into the field of view by adjusting the counterbalance voltage using a feedback loop, a process that took ~3 s on average. Thus, far-field imaging tracked merging events for time scales of <3 s, as seen in fig. S1B. The far-field images analysis is a template-based autocorrelation of the far-field images, where the template image was the original image offset in the horizontal (x) direction, as described elsewhere (*14*). Far-field images were recorded and then post-processed in LabVIEW. An image within the recorded sequence was duplicated and then offset horizontally in the x-direction by n pixels (n = 20 pixels, typically). The absolute difference between the overlapping pixel values of the offset image and the original image created a "defect" image. The average defect image intensity $\bar{I}_D$ was normalized to the average far-field intensity $\bar{I}$ of the original image to calculate a correlation value C, given in Eq. 1

$$C = (\bar{I} - \bar{I}_D)/\bar{I} \quad (1)$$

Tracking the correlation value as a function of time was used to monitor coalescence events at time scales of <3 s (*14*).

Materials

All chemicals were purchased from Sigma-Aldrich (>99% purity) except *N*-acetylneuraminic acid (Alfa Aesar; 97% purity). Stock solutions were 5 wt %, made from Millipore water (18 megohms), and filtered before dispensing. Fresh solutions were made daily. The pH of the solutions was not adjusted, and the pH for a 5–wt % 1:1 (by mole) $CaCl_2$-organic stock solution was ~3 for the carboxylic acids and ~6 for neutral organics. The pH of levitated droplets was unknown.

Statistical analysis

Droplets were merged for a minimum of three to five times at a constant RH (ΔRH of <1 to 2% typical because of temporal variations), with average τ or t_{obs} reported in Figs. 2 and 3 with ±1 SD and average RH (±1 SD) reported with propagated error from individual RH measurements, where an individual RH measurement was the average reading (±1 SD) of RH probes at the inlet and outlet. The absolute uncertainty in the RH probes is ±2% RH. This uncertainty was not propagated into the reported uncertainty. Additional uncertainty exists in the viscosity and mole fraction of water because of slow equilibration with ambient RH. This uncertainty is not well

quantified and is not included in the uncertainty shown in Fig. 2 and fig. S2. Typical uncertainty from a 5-min equilibration time scale is ~1 order of magnitude (*14*), which is common for measurements of viscosity that span 10 orders of magnitude (*14*, *17*).

Raman spectroscopy

Raman spectra were obtained to compare the relative water content of binary gluconic acid droplets to that of ternary $CaCl_2$:gluconic acid droplets (fig. S5B) and to examine for spectral evidence of ion pairing (fig. S8). Spectra were collected using a 532-nm laser as the excitation source. As shown in fig. S1A, the laser illuminated the droplets from below. Laser light was gently focused onto the droplets with a 200-mm focal length lens. The laser power was ~500 mW in total. Scattered light was collected perpendicular to the laser axis. The Rayleigh scattered light was removed with a notch filter, and inelastically scattered light focused onto a fiber optic coupled to a spectrometer (Princeton Instruments, Fergie FER-SCI-BRX; 1200 g/mm grating). Spectra were collected with an exposure time of 5 s, and eight spectra were averaged.

Thermodynamic modeling

The web-based version of the AIOMFAC model (AIOMFAC-web; https://aiomfac.lab.mcgill.ca) (*27*, *29*) was used to estimate the water content of binary and ternary droplets (Figs. 2, F to I, and 3B) and to estimate whether the binary organics were predicted to exhibit a glass transition. The organic molecules were defined in AIOMFAC in their linear form. For binary *N*-acetylneuraminic acid, AIOMFAC cannot fully define the acetylamino group. Thus, the acetylamino functional group was approximated as a secondary amine and a ketone. This approximation was used for *N*-acetylneuraminic acid to predict RH-dependent viscosity, which is a practical assumption considering the dependence of viscosity on molecular mass (*19*), but was not used to predict water content in ternary mixtures. Thus, Fig. 2 does not show viscosity as a function of water mole fraction for *N*-acetylneuraminic acid systems.

RH oscillation measurements

Droplets were held in a linear quadrupole EDB (*35*) (functionally equivalent to the DBQ-EDB) and exposed to a sinusoidal oscillation in RH with a controlled frequency (*34*). The response of the droplet was monitored from whispering gallery modes excited by light-emitting diode illumination and measured using an Ocean Optics HR4000+ spectrometer (*35*). The amplitude of the droplet response was determined at each frequency, and the relative response of the droplet was found by comparison to the maximum amplitude. The half-time response of the droplet was determined at each RH using a sigmoid fit to the response as a function of time period (1 / frequency).

DC balance mass measurements

In the absence of air flow, the only force contributing to the DC balance voltage (V_{DC}) needed for levitation is the force of gravity (mass). Thus, changes in V_{DC} can be directly attributed to changes in droplet mass, as water is lost. To measure the relative change in mass of droplets as a function of RH, droplets were held in the bottom balance at an initial RH for 15 min. The air flow was momentarily switched off (<2 s), and the initial DC balance voltage ($V_{DC,i}$) necessary to levitate the droplet was recorded. The RH was then reduced by 5 to 7% RH, the droplet was equilibrated for 15 min, and V_{DC} was recorded again. The relative change in mass at each RH was found as $V_{DC}(RH)$ / $V_{DC,i}$ where $V_{DC}(RH)$ is the V_{DC} reading at a specific RH.

SUPPLEMENTARY MATERIALS

Supplementary material for this article is available at http://advances.sciencemag.org/cgi/content/full/6/47/eabb5643/DC1

REFERENCES AND NOTES

1. M. V. Orellana, P. A. Matrai, C. Leck, C. D. Rauschenberg, A. M. Lee, E. Coz, Marine microgels as a source of cloud condensation nuclei in the high arctic. *Proc. Natl. Acad. Sci.* **108**, 13612–13617 (2011).
2. R. E. Cochran, O. Laskina, J. V. Trueblood, A. D. Estillore, H. S. Morris, T. Jayarathne, C. M. Sultana, C. Lee, P. Lin, J. Laskin, A. Laskin, J. A. Dowling, Z. Qin, C. D. Cappa, T. H. Bertram, A. V. Tivanski, E. A. Stone, K. A. Prather, V. H. Grassian, Molecular diversity of sea spray aerosol particles: Impact of ocean biology on particle composition and hygroscopicity. *Chem* **2**, 655–667 (2017).
3. Q. Mu, M. Shiraiwa, M. Octaviani, N. Ma, A. Ding, H. Su, G. Lammel, U. Pöschl, Y. Cheng, Temperature effect on phase state and reactivity controls atmospheric multiphase chemistry and transport of PAHs. *Sci. Adv.* **4**, eaap7314 (2018).
4. R. D. Davis, M. A. Tolbert, Crystal nucleation initiated by transient ion-surface interactions at aerosol interfaces. *Sci. Adv.* **3**, e1700425 (2017).
5. E. Mikhailov, S. Vlasenko, S. T. Martin, T. Koop, U. Poschl, Amorphous and crystalline aerosol particles interacting with water vapor: Conceptual framework and experimental evidence for restructuring, phase transitions and kinetic limitations. *Atmos. Chem. Phys.* **9**, 9491–9522 (2009).
6. J. P. Reid, A. K. Bertram, D. O. Topping, A. Laskin, S. T. Martin, M. D. Petters, F. D. Pope, G. Rovelli, The viscosity of atmospherically relevant organic particles. *Nat. Commun.* **9**, 956 (2019).
7. S. S. Petters, S. M. Kreidenweis, A. P. Grieshop, P. J. Ziemann, M. D. Petters, Temperature- and humidity-dependent phase states of secondary organic aerosols. *Geophys. Res. Lett.* **46**, 1005–1013 (2019).
8. M. Shiraiwa, Y. Li, A. P. Tsimpidi, V. A. Karydis, T. Berkemeier, S. N. Pandis, J. Lelieveld, T. Koop, U. Pöschl, Global distribution of particle phase state in atmospheric secondary organic aerosols. *Nat. Commun.* **8**, 15002 (2017).
9. T. Koop, J. Bookhold, M. Shiraiwa, U. Pöschl, Glass transition and phase state of organic compounds: Dependency on molecular properties and implications for secondary organic aerosols in the atmosphere. *Phys. Chem. Chem. Phys.* **13**, 19238–19255 (2011).
10. Y. You, L. Renbaum-Wolff, A. K. Bertram, Liquid–liquid phase separation in particles containing organics mixed with ammonium sulfate, ammonium bisulfate, ammonium nitrate or sodium chloride. *Atmos. Chem. Phys.* **13**, 11723–11734 (2013).
11. J. L. Jimenez, M. R. Canagaratna, N. M. Donahue, A. S. H. Prevot, Q. Zhang, J. H. Kroll, P. F. De Carlo, J. D. Allan, H. Coe, N. L. Ng, A. C. Aiken, K. S. Docherty, I. M. Ulbrich, A. P. Grieshop, A. L. Robinson, J. Duplissy, J. D. Smith, K. R. Wilson, V. A. Lanz, C. Hueglin, Y. L. Sun, J. Tian, A. Laaksonen, T. Raatikainen, J. Rautiainen, P. Vaattovaara, M. Ehn, M. Kulmala, J. M. Tomlinson, D. R. Collins, M. J. Cubison, E. J. Dunlea, J. A. Huffman, T. B. Onasch, M. R. Alfarra, P. I. Williams, K. Bower, Y. Kondo, J. Schneider, F. Drewnick, S. Borrmann, S. Weimer, K. Demerjian, D. Salcedo, L. Cottrell, R. Griffin, A. Takami, T. Miyoshi, S. Hatakeyama, A. Shimono, J. Y. Sun, Y. M. Zhang, K. Dzepina, J. R. Kimmel, D. Sueper, J. T. Jayne, S. C. Herndon, A. M. Trimborn, L. R. Williams, E. C. Wood, A. M. Middlebrook, C. E. Kolb, U. Baltensperger, D. R. Worsnop, Evolution of organic aerosols in the atmosphere. *Science* **326**, 1525–1529 (2009).
12. L. M. Russell, L. N. Hawkins, A. A. Frossard, P. K. Quinn, T. S. Bates, Carbohydrate-like composition of submicron atmospheric particles and their production from ocean bubble bursting. *Proc. Natl. Acad. Sci.* **107**, 6652–6657 (2010).
13. J. F. Davies, K. R. Wilson, Raman spectroscopy of isotopic water diffusion in ultraviscous, glassy, and gel states in aerosol by use of optical tweezers. *Anal. Chem.* **88**, 2361–2366 (2016).
14. D. S. Richards, K. Trobaugh, J. Hajek-Herrera, R. D. Davis, Dual-balance electrodynamic trap as a micro-analytical tool for identifying gel transitions and viscous properties of levitated aerosol particles. *Anal. Chem.* **92**, 3086–3094 (2020).
15. G. Rovelli, Y.-C. Song, A. M. Maclean, D. O. Topping, A. K. Bertram, J. P. Reid, Comparison of approaches for measuring and predicting the viscosity of ternary component aerosol particles. *Anal. Chem.* **91**, 5074–5082 (2019).
16. A. Marsh, S. S. Petters, N. E. Rothfuss, G. Rovelli, Y. C. Song, J. P. Reid, M. D. Petters, Amorphous phase state diagrams and viscosity of ternary aqueous organic/organic and inorganic/organic mixtures. *Phys. Chem. Chem. Phys.* **20**, 15086–15097 (2018).
17. Y. C. Song, A. E. Haddrell, B. R. Bzdek, J. P. Reid, T. Bannan, D. O. Topping, C. Percival, C. Cai, Measurements and predictions of binary component aerosol particle viscosity. *J. Phys. Chem.* **120**, 8123–8137 (2016).
18. R. M. Power, S. H. Simpson, J. P. Reid, A. J. Hudson, The transition from liquid to solid-like behaviour in ultrahigh viscosity aerosol particles. *Chem. Sci.* **4**, 2597–2604 (2013).

19. J. W. Grayson, E. Evoy, M. Song, Y. Chu, A. Maclean, A. Nguyen, M. A. Upshur, M. Ebrahimi, C. K. Chan, F. M. Geiger, R. J. Thomson, A. K. Bertram, The effect of hydroxyl functional groups and molar mass on the viscosity of non-crystalline organic and organic–water particles. *Atmos. Chem. Phys.* **17**, 8509–8524 (2017).
20. A. Marsh, G. Rovelli, R. E. H. Miles, J. P. Reid, Complexity of measuring and representing the hygroscopicity of mixed component aerosol. *J. Phys. Chem.* **123**, 1648–1660 (2019).
21. Y. Kim, K. Sartelet, F. Couvidat, Modeling the effect of non-ideality, dynamic mass transfer and viscosity on SOA formation in a 3-D air quality model. *Atmos. Chem. Phys.* **19**, 1241–1261 (2019).
22. M. V. Orellana, P. Verdugo, Ultraviolet radiation blocks the organic carbon exchange between the dissolved phase and the gel phase in the ocean. *Limnol. Oceanogr.* **48**, 1618–1623 (2003).
23. S. R. Schill, S. M. Burrows, E. S. Hasenecz, E. A. Stone, T. H. Bertram, The impact of divalent cations on the enrichment of soluble saccharides in primary sea spray aerosol. *Atmosphere* **9**, 476 (2018).
24. Y.-H. Zhang, C. K. Chan, Study of contact ion pairs of supersaturated magnesium sulfate solutions using raman scattering of levitated single droplets. *J. Phys. Chem.* **104**, 9191–9196 (2000).
25. K. Y. Lee, D. J. Mooney, Alginate: Properties and biomedical applications. *Prog. Polym. Sci.* **37**, 106–126 (2012).
26. J. Buajarern, L. Mitchem, J. P. Reid, Manipulation and characterization of aqueous sodium dodecyl sulfate/sodium chloride aerosol particles. *J. Phys. Chem.* **111**, 13038–13045 (2007).
27. N. R. Gervasi, D. O. Topping, A. Zuend, A predictive group-contribution model for the viscosity of aqueous organic aerosol. *Atmos. Chem. Phys.* **20**, 2987–3008 (2020).
28. E. M. Adams, B. A. Wellen, R. Thiraux, S. K. Reddy, A. S. Vidalis, F. Paesani, H. C. Allen, Sodium–carboxylate contact ion pair formation induces stabilization of palmitic acid monolayers at high pH. *Phys. Chem. Chem. Phys.* **19**, 10481–10490 (2017).
29. A. Zuend, C. Marcolli, A. M. Booth, D. M. Lienhard, V. Soonsin, U. K. Krieger, D. O. Topping, G. McFiggans, T. Peter, J. H. Seinfeld, New and extended parameterization of the thermodynamic model AIOMFAC: Calculation of activity coefficients for organic-inorganic mixtures containing carboxyl, hydroxyl, carbonyl, ether, ester, alkenyl, alkyl, and aromatic functional groups. *Atmos. Chem. Phys.* **11**, 9155–9206 (2011).
30. Y. Li, T. Tanaka, Phase transitions of gels. *Ann. Rev. Mater. Sci.* **22**, 243–277 (1992).
31. K. M. Galler, L. Aulisa, K. R. Regan, R. N. D'Souza, J. D. Hartgerink, Self-assembling multidomain peptide hydrogels: Designed susceptibility to enzymatic cleavage allows enhanced cell migration and spreading. *J. Am. Chem. Soc.* **132**, 3217–3223 (2010).
32. M. Laliberté, Model for calculating the viscosity of aqueous solutions. *J. Chem. Eng. Data* **52**, 321–335 (2007).
33. P. Verdugo, Marine microgels. *Ann. Rev. Mar. Sci.* **4**, 375–400 (2012).
34. T. Preston, J. F. Davies, K. R. Wilson, The frequency-dependent response of single aerosol particles to vapour phase oscillations and its application in measuring diffusion coefficients. *Phys. Chem. Chem. Phys.* **19**, 3922–3931 (2017).
35. C. L. Price, A. Bain, B. J. Wallace, T. C. Preston, J. F. Davies, Simultaneous retrieval of the size and refractive index of suspended droplets in a linear quadrupole electrodynamic balance. *J. Phys. Chem. A* **124**, 1811–1820 (2020).
36. G. Pasin, G. G. Birch, Calcium chloride complex formation of glucose syrups and their fractions. *Food Chem.* **19**, 149–158 (1986).
37. M. C. R. Symons, J. A. Benbow, H. Pelmore, Interactions between calcium ions and a range of monosaccharides studied by hydroxy-proton resonance spectroscopy. *J. Chem. Soc. Faraday Transl.* **80**, 3671–3677 (1999).
38. P. Lo Nostro, B. W. Ninham, S. Milani, L. Fratoni, P. Baglioni, Specific anion effects on the optical rotation of glucose and serine. *Biopolymers* **81**, 136–148 (2006).
39. H.-A. Tajmir-Riahi, Sugar interaction with calcium ion. Synthesis and vibrational spectra of crystalline β-D-fructose and its calcium halide adducts. *J. Inorganic Biochem.* **27**, 123–131 (1986).
40. B. A. W. Rudd, A. S. Vidalis, H. C. Allen, Thermodynamic *versus* non-equilibrium stability of palmitic acid monolayers in calcium-enriched sea spray aerosol proxy systems. *Phys. Chem. Chem. Phys.* **20**, 16320–16332 (2018).
41. Y. Zhang, S. Furyk, D. E. Bergbreiter, P. S. Cremer, Specific ion effects on the water solubility of macromolecules: PNIPAM and the Hofmeister series. *J. Am. Chem. Soc.* **127**, 14505–14510 (2005).
42. H. Oertling, Interactions of alkali- and alkaline earth-halides with carbohydrates in the crystalline state – the overlooked salt and sugar cocrystals. *CrstEngComm* **18**, 1676–1692 (2016).
43. D. T. Shindell, J.-F. Lamarque, M. Schulz, M. Flanner, C. Jiao, M. Chin, P. J. Young, Y. H. Lee, L. Rotstayn, N. Mahowald, G. Milly, G. Faluvegi, Y. Balkanski, W. J. Collins, A. J. Conley, S. Dalsoren, R. Easter, S. Ghan, L. Horowitz, X. Liu, G. Myhre, T. Nagashima, V. Naik, S. T. Rumbold, R. Skeie, K. Sudo, S. Szopa, T. Takemura, A. Voulgarakis, J.-H. Yoon, F. Lo, Radiative forcing in the ACCMIP historical and future climate simulations. *Atmos. Chem. Phys.* **13**, 2939–2974 (2013).
44. S. B. Clough, H. E. Read, A. B. Metzner, V. C. Behn, Diffusion in slurries and in non-Newtonian fluids. *AIChE J.* **8**, 346–350 (1962).
45. B. Jing, Z. Wang, F. Tan, Y. Guo, S. Tong, W. Wang, Y. Zhang, M. Ge, Hygroscopic behavior of atmospheric aerosols containing nitrate salts and water-soluble organic acids. *Atmos. Chem. Phys.* **18**, 5115–5127 (2018).
46. N. E. Olson, Z. Lei, R. L. Craig, Y. Zhang, Y. Chen, A. T. Lambe, Z. Zhang, A. Gold, J. D. Surratt, A. P. Ault, Reactive uptake of isoprene epoxydiols increases the viscosity of the core of phase-separated aerosol particles. *ACS Earth Space Chem.* **3**, 1402–1414 (2019).
47. A. Virtanen, J. Joutsensaari, T. Koop, J. Kannosto, P. Yli-Pirilä, J. Leskinen, J. M. Mäkelä, J. K. Holopainen, U. Pöschl, M. Kulmala, D. R. Worsnop, A. Laaksonen, An amorphous solid state of biogenic secondary organic aerosol particles. *Nature* **467**, 824–827 (2010).

Acknowledgments: We thank M. Jacobs and K. Wilson for assistance with the DBQ-EDB, G. Rovelli for constructive feedback on the manuscript, C. Pursell for assistance with the Raman setup, A. Zuend for advice with AIOMFAC, and A. Urbach for discussion on supramolecular interactions. **Funding:** This work was supported by Trinity University startup funds, and the work related to aerosol viscosity and particle merging is supported by the National Science Foundation (grant AGS-1925208). D.S.R. acknowledges a Murchison Undergraduate Research Fellowship. K.L.T. and J.H.-H. acknowledge support from the Welch Foundation (grant W-0031). J.F.D. acknowledges support from UC Riverside startup funds for the RH oscillation experiments. **Author contributions:** D.S.R. performed experiments, analyzed data, constructed equipment, and wrote portions of the manuscript. K.L.T. performed experiments, analyzed data, and constructed equipment. J.H.-H. performed experiments and constructed equipment. C.L.P., C.S.S., and J.F.D. performed RH oscillation experiments, analyzed data, and wrote portions of the manuscript. R.D.D. designed the research, performed experiments, analyzed data, and wrote the manuscript. All authors read and commented on the manuscript. **Competing interests:** The authors declare that they have no competing interests. All authors read and commented on the manuscript. **Data and materials availability:** All data needed to evaluate the conclusions in the paper are present in the paper and/or the Supplementary Materials. Additional data related to this paper may be requested from the authors.

Submitted 12 March 2020
Accepted 7 October 2020
Published 18 November 2020
10.1126/sciadv.abb5643

Citation: D. S. Richards, K. L. Trobaugh, J. Hajek-Herrera, C. L. Price, C. S. Sheldon, J. F. Davies, R. D. Davis, Ion-molecule interactions enable unexpected phase transitions in organic-inorganic aerosol. *Sci. Adv.* **6**, eabb5643 (2020).

Science Advances

Ion-molecule interactions enable unexpected phase transitions in organic-inorganic aerosol

David S. Richards, Kristin L. Trobaugh, Josefina Hajek-Herrera, Chelsea L. Price, Craig S. Sheldon, James F. Davies and Ryan D. Davis

Sci Adv **6** (47), eabb5643.
DOI: 10.1126/sciadv.abb5643